ZrO$_2$−SiO$_2$ Nanosheets with Ultrasmall WO$_3$ Nanoparticles and Their Enhanced Pseudocapacitance and Stability
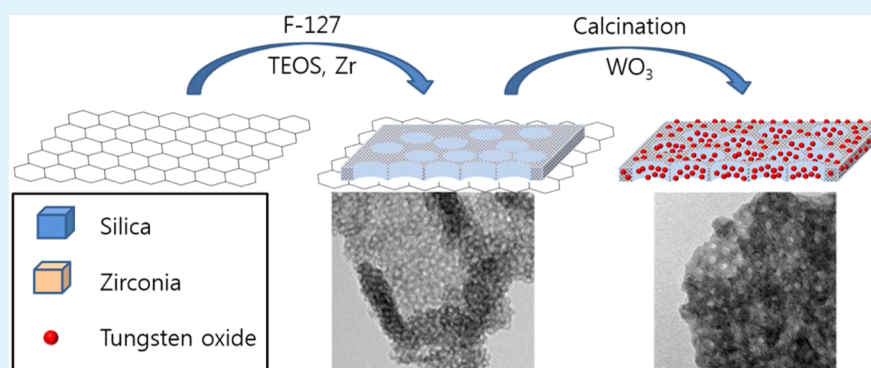
Gyoung Hwa Jeong,[†,‡] Hae-Min Lee,[†,⊥] Ji-goo Kang,[§] Heewoong Lee,[§] Chang-Koo Kim,[⊥] Jae-Hyeok Lee,[§] Jae-Ho Kim,[§] and Sang-Wook Kim*,[‡,§]

[‡]Center of Molecular Science and Technology, [⊥]Division of Energy Systems Research, and [§]Department of Molecular Science and Technology, Ajou University, Suwon 443-749, Korea

S *Supporting Information*

ABSTRACT: We report on the first synthesis of porous ZrO$_2$−SiO$_2$ sheets with well-defined ultrasmall WO$_3$ nanoparticles for energy storage performance. In our system, for improving the surface deterioration of electrode, we use the ZrO$_2$−SiO$_2$ sheets using graphene oxide as a template to access electrode substrate. The synthesized electrode with about 20 nm thickness and about 10 nm pores, has a maximum value of 313 F/g at current density of 1 A/g and a minimum value of 160 F/g at current density of 30 A/g in the specific capacitance. In addition, over 90% of its initial specific capacitance is retained when they are cycled up to 2500 cycles.

KEYWORDS: *porous sheets, WO$_3$ nanoparticle, supercapacitor, stability*

1. INTRODUCTION

Supercapacitors have attracted interest in the field of next-generation electrical energy storage because of their various properties such as high energy density, high power density, low equivalent series resistance, and long charge−discharge life.[1−3] In general, supercapacitors can be classified as electrochemical double layer capacitors (EDLCs) and pseudocapacitors, depending on the nature of the above-mentioned interfacial processes. EDLCs are charged by the reversible adsorption of ions on the electrode and electrolyte interface of the carbon-based materials with high surface area such as activated carbon, carbon nanotubes (CNTs), aerogels, and graphene,[4−6] whereas pseudocapacitors are charged by conducting redox reactions on the surface of the electrodes such as metal oxides, including RuO$_2$, Fe$_3$O$_4$, Co$_3$O$_4$, and NiO[7−10] or by using conducting polymers.[11] It is well-known that pseudocapacitors can provide higher specific capacitance and energy density than EDLCs.[12] For example, RuO$_2$ and MnO$_2$ have a theoretical specific capacitance of 1340 F/g and 1300 F/g in aqueous electrolytes, respectively.[12] However, they have a low electrical conductance, poor compatibility with organic electrolytes, and poor stability during the cycling process because of the redox reaction of metal oxides.[13] Therefore, it is still difficult to synthesize highly stable and low-cost metal oxides with various structures.

Graphene is the one of the most-studied carbon-based electrode materials because of the large surface area, high intrinsic electrical conductivity, high mechanical strength, high chemical stability, and low cost compared with single-walled CNTs.[14−17] Metal oxides/graphene composites are mostly derived by the chemical reduction of graphite oxide (GO) using strong reductants.[18,19] However, the use of reduced GO poses a problem; its use causes aggregation of graphene layers during chemical reduction. This restacking hinders the access of the electrolyte ions to the surface of the reduced GO and decreases the surface area. To resolve this restacking, graphene based composites with various metal oxide nanoparticles (NPs) such as Ni(OH)$_2$,[20] Mn$_3$O$_4$,[21] MnO$_2$,[22] and Co$_3$O$_4$[23] have been frequently reported. However, although all these graphene based composites yielded enhanced specific capacitance, it is not sufficient for practical applications; we still face problems
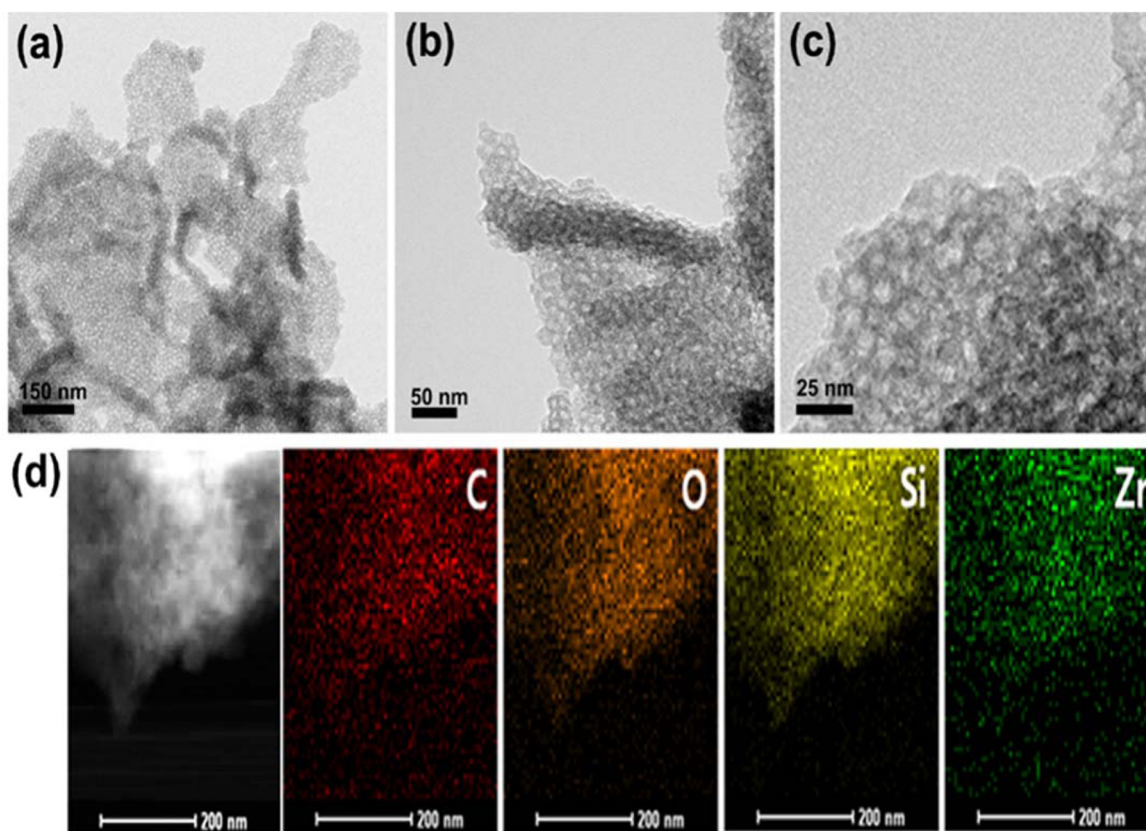
Figure 1. (a−c) TEM images of porous ZrO_2−SiO_2 NSs on the GO. (d) HAADF-STEM mapping images of porous ZrO_2−SiO_2 NSs on the GO.

caused by restacking and the remaining oxygen ligands of graphene.

Herein, we tried to improve the stability of electrode materials by focusing on the other part of graphene or GO as a substrate with a two-dimensional (2D) sheet structure. This 2D structure was recently considered as a template for controlling the shape of electrode materials.[24−35] In particular, porous SiO_2 nanosheets (NSs) are advantageous for synthesis as well as applications of nanomaterials.[27−35] For example, the partial phase transformation of SiO_2-carbon composites from the 2D hexagonal structure into the lamellar phase is induced by graphene sheets at high temperature.[34] In addition, graphene-NS-supported ultrafine metal NPs encapsulated by thin mesoporous SiO_2 layers were prepared and used as robust catalysts with high catalytic activity and excellent high temperature stability in the fields of CO oxidation and reduction reactions.[29] However, in present, these most reported materials uses in only acting as molds for new materials synthesis, organic catalysts, low dielectronic coatings, and optical materials. It is well-known that binary composite oxides such as ZrO_2−SiO_2 are important to fabricate materials with chemical, thermal, and mechanical stabilities.[36,37] However, these binary composite oxides have relatively low surface areas. To overcome this shortcoming, we synthesized new ternary oxide system of porous ZrO_2−SiO_2 sheets with ultrasmall WO_3 NPs for the energy-storage device. WO_3 is an attractive electrode materials because of its multiple oxidation states. Nevertheless, there are rarely reports on the capacitive performance of WO_3. Therefore, in our system, ultrasmall WO_3 NPs is synthesized on the porous ZrO_2−SiO_2 sheets by the impregnation. The synthesized electrode material is approximately 20 nm thick, had 10 nm pores, and had a

maximum specific capacitance of 313 F/g at a current density of 1 A/g and a minimum specific capacitance of 160 F/g at a current density of 30 A/g. In addition, over 90% of its initial specific capacitance was retained when an electrode comprising ZrO_2−SiO_2 NS with ultrasmall WO_3 NPs was cycled up to 2500 cycles.

2. EXPERIMENTAL SECTION

Chemicals. Graphite powder, hydrochloric acid (HCl, 35.0−37.0%), and sulfuric acid (H_2SO_4, 95%) were obtained from SAMCHUN Chemicals (Korea). Pluronic F-127 ($PEO_{106}PPO_{70}PEO_{106}$, M_w = 12600), tetraethylorthosilicate (TEOS, 98%), and sucrose (Grade II) were purchased from Sigma-Aldrich. Sodium hydroxide (NaOH, 98%) was obtained from OCI Company. Ammonium metatungstate hydrate (($NH4)_6H_2W_{12}O_{40}$·xH_2O, 99.99%) was acquired from Aldrich. All the chemicals were used as received without any further purification. The aqueous solutions were prepared using ultrapure water (Milli-Q, Millipore).

Synthesis of Porous ZrO_2−SiO_2 NS with Ultrasmall WO_3 NPs. GO as a template was synthesized using graphite powder by Hummers method.[33] In this typical experiment, as-synthesized GO (30 mg) and 50 mL of deionized water mixture was ultrasonically treated for 0.5 h in an ice bath. Pluronic F-127 was dissolved in 50 mL of water, and then added to the mixture. Subsequently, the ultrasonic treatment was applied to the mixture for 1 h and 30 min. To remove the precipitates, the mixture was centrifuged for 20 min at 3400 rpm. Then, 0.3 mL of 10% HCl/water solution was added to the supernatant. The above mixture was heated at 80 °C for 1 h and 20 min. Next, 868.8 mg of TEOS and was gradually added dropwise to the mixture at 80 °C, and the resulting mixture was again heated at 80 °C for 24 h and cooled at room temperature. The product was washed with ethanol and dried overnight at 120 °C in a conventional oven. And then the W precursor (($NH4)_6H_2W_{12}O_{40}$·xH_2O) was dissolved in deionized water. This W aqua solution was impregnated to the prepared templates. The mixture
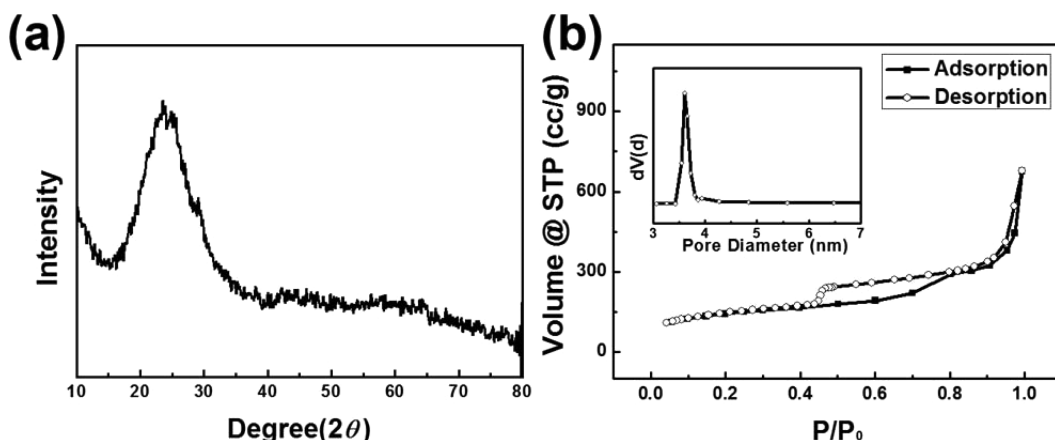
Figure 2. (a)XRD pattern of porous ZrO_2-SiO_2 NSs on GO. (b) Nitrogen adsorption/desorption isotherms and BJH pore distribution (inset) of porous ZrO_2-SiO_2 NSs on the GO.

was dried at 120 °C for 3 h and calcined at 550 °C for 6 h under atmosphere system (heating rate was 1 °C/min).

Synthesis of Electrode. A ZrO_2-SiO_2 NS with ultrasmall WO_3 NP electrode was prepared by using the active material, Super P carbon black (MMM carbon), and polytetrafluoroethylene (PTFE) binder in 65:25:10 weight ratio. The mixture was loaded onto a 110 μm thick Ni foil by using 10 wt % PTFE (60 wt % dispersion in water, Sigma-Aldrich) as a binder. The mixture of the synthesized powder and Super P carbon black was homogenized in an agate mortar and formed into electrodes by rolling the mixture into 50-μm-thick sheets. The mixture-coated electrode was dried in an oven at 80 °C for 6 h. To investigate the effect of WO_3 for electrochemical performance, we also prepared ZrO_2-SiO_2 NSs mixed with the carbon electrode on a Ni foil in the same way.

Electrochemical Characterization. The electrochemical properties were characterized out using a standard three-electrode cell at room temperature (24 ± 1 °C) by using a computer-controlled potentiostat (Princeton Applied Research, VSP). A saturated Ag/AgCl electrode and a platinum-coated titanium mesh (2.5 cm² in size) were used as reference and counter electrodes, respectively. A modified glassy carbon electrode (diameter 3 mm) was used as the working electrode, and 2 M KCl as the electrolyte. Before electrochemical analysis, the electrolyte was deaerated by nitrogen gas for 5 min. The cyclic voltammograms (CVs) were recorded between −1.3 and 1.1 V vs Ag/AgCl at a scan rate 100 mV/s. The constant current charge/discharge reaction was carried out chrono-potentiometrically by varying the charge/discharge current from 1 to 30A/g. The electrode was discharged to −1.2 V (at the fully discharged state) in the first cycle and charged to 1.1 V (at the fully charged state) in the second cycle. The specific capacitance (C_{sp}) was calculated from the charge/discharge curves as follows

$$C_{sp} = \frac{dQ}{dVm} = \frac{I_{cons}}{(dV/dt)m} \quad (1)$$

where Q is the charge on the electrode, I_{cons} is the constant current in ampere, dV/dt was calculated from the slope of the discharge curve in volts per second (V/s), and m is the mass of active material.

Characterization. X-ray diffraction (XRD) patterns were obtained with a RigakuUltima III diffractometer, equipped with a rotating anode and a Cu−Kαradiation source (λ = 0.15418 nm). The transmission electron microscopy (TEM) and scanning transmission electron microscopy (STEM) images were taken on a FEI Tecnai G2 F30 Super-Twin transmission electron microscope operating at 300 kV. The TEM sample was prepared on a copper grid coated with an amorphous carbon film. The STEM sample was prepared on a microcopper grid without any supporting film (JEOL-780111613). The thickness value was obtained by operating the Park Systems XE-100 atomic force microscope in the noncontact mode. The values of adsorption/desorption isotherm, specific surface area, and pore-size

distribution were achieved by using the Quantachrome Instruments QUADRASORB SI gas adsorption/desorption analyzer operating at 77 K. The specific surface area was calculated by the Brunauer−Emmett−Teller (BET) method and pore-size distribution was calculated by the Barrett−Joyner−Halenda (BJH) method.

3. RESULTS AND DISCUSSION

Recently, Yang et al.[33] showed mesoporous GO-silica NSs using cetyltrimethylammonium bromide (CTAB) as a cation surfactant. The resulting product was observed containing multiple free-standing 200 nm to several micrometers long sheets with morphology similar to that of graphene. We performed a similar experiment using a nonionic surfactant instead of CTAB; we could also observe the 2D ZrO_2-SiO_2 sheets with large area on the GO surface (see the TEM images in Figure 1a, b and Figure S1 in the Supporting Information). Pluronic F-127, which is used as the nonionic surfactant, has a polymeric PEO−PPO structure; as a result, the large pore of the synthesized sheets is approximately 13 nm compared with those of the sheets obtained using CTAB. Most of the reported porous SiO_2 sheet materials stated in the Introduction section use CTAB as the pore-generating agent, and have pores of approximately 2 nm (Figure 1b and Figure S2 in the Supporting Information). Pluronic F-127 has a high molecular weight with a large hydrophilic volume, offering the possibility of the formation of mesoporous oxides with thick walls that may increase the thermal and hydrothermal stability.[38] To confirm the layered composite structure of GO and ZrO_2-SiO_2 NSs, we used high-angle annular dark-field scanning TEM (HAADF-STEM) (Figure 1d). From the nanoscale element-mapping images, we could investigate that the distributions of Zr, Si, and carbon are equal in the chosen field, confirming the presence of porous ZrO_2-SiO_2 NSs on the GO surface. From the atomic force microscopy (AFM), we observed that the synthesized graphene composites are approximately 12.5 nm thick (see Figure S3 in the Supporting Information).

The XRD pattern shows the structural characteristics of porous ZrO_2-SiO_2 NSs on the GO (Figure 2a). A tiny peak around 30°, which resulted from the low mole ratio (1/10) of Zr and Si precursors, indicates the presence of the tetragonal ZrO_2 structure and broad weak feature between 2θ = 20 and 40° and is the evidence of amorphous SiO_2. Figure 2b shows the nitrogen adsorption/desorption isotherms and BJH pore distribution, which show type IV characteristics. Surface area and pore volume are calculated by the BET method. The
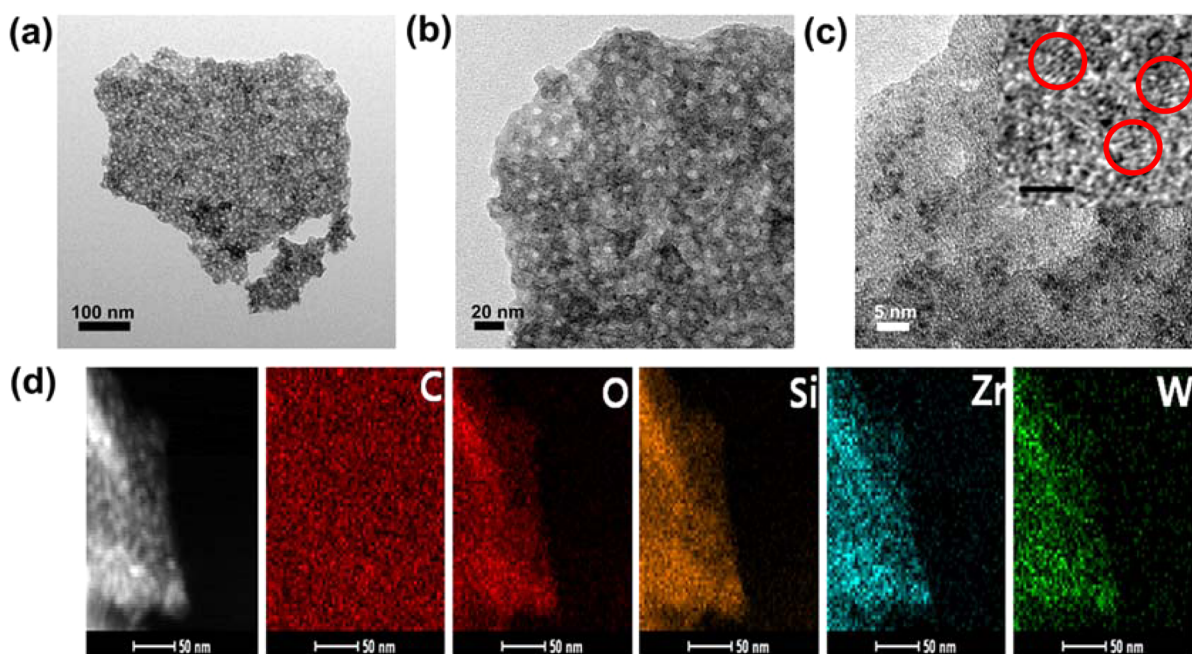
Figure 3. (a−c) TEM images of porous ZrO$_2$−SiO$_2$ NSs with ultrasmall WO$_3$ nanoparticles after calcination. Scale bar in inset of c is 2 nm. (d) HAADF-STEM mapping images of porous ZrO$_2$−SiO$_2$ NSs.
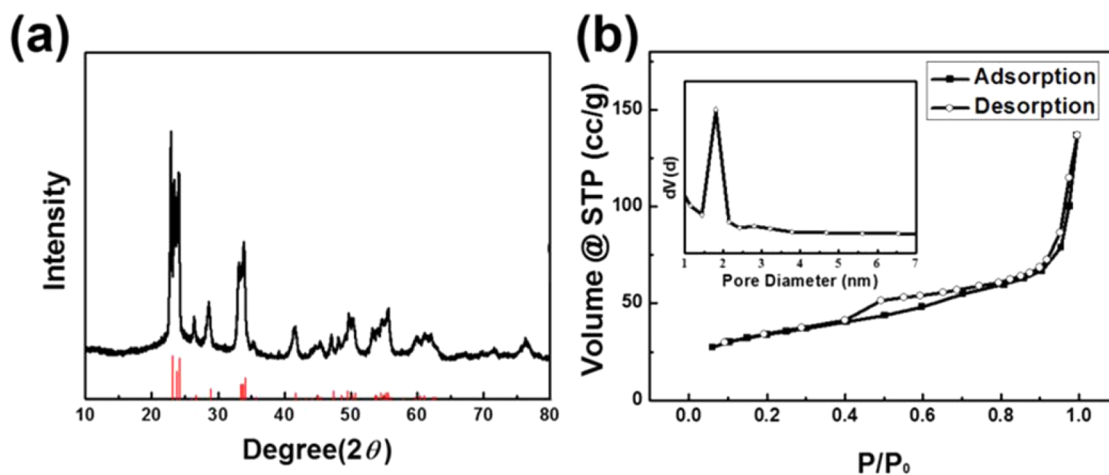
**Figure 4.** (a)XRD pattern of porous ZrO$_2$−SiO$_2$ NSs NSs with ultrasmall WO$_3$ nanoparticles. (b) Nitrogen adsorption/desorption isotherms and BJH pore distribution (inset) of porous ZrO$_2$−SiO$_2$ NSs with ultrasmall WO$_3$ nanoparticles.

surface area and pore size of the synthesized NSs are 515.19 m^2/g and 3.6 nm, respectively. Interestingly, there is a difference in the pore size values obtained by TEM images (Figure 1) and that by isotherm data. A possible reason is that 13 nm sized pore which is observed by TEM is too open a shape to be measured by the nitrogen adsorption/desorption because no condensation of gas occurred on the surface[31] (see the thickness of NSs on GO is approximatively 15 nm, see Figure S3 in the Supporting Information). The 3.6 nm pore, which is supposed to be located on the wall, is not detected by TEM. As a control experiment, the formation of a ZrO$_2$−SiO$_2$ NS was tried in the absence of GO. As shown in Figure S4 in the Supporting Information, the NSs were not synthesized under this condition, which shows that the GO is a good template.

After impregnating a W precursor in porous ZrO$_2$−SiO$_2$ NSs on the GO, it was calcined at 500 °C for 5 h under atmosphere.

Consequently, we were able to obtain porous ZrO$_2$−SiO$_2$ NS with ultrasmall WO$_3$ NPs without GO. Figure 3 shows the TEM images of the porous NS with ultrasmall WO$_3$ NPs. These images show that WO$_3$ NPs with approximately 1.5 nm size are well distributed on the surface; interestingly, the framework structure gets changed. Moreover, large pores of 13 nm size are diminished to approximately 5 nm and the framework wall is thickened more. As shown in the HR-TEM image (Figure 3c), WO$_3$ NPs positioned into the framework of porous ZrO$_2$−SiO$_2$ NS. WO$_3$ NPs the lattice planes are approximately 0.236 nm corresponding to the interplanar distance of the WO$_3$ (011) plane. Generally, the size of the impregnated metal or metal oxide NPs is similar to the pore size of the materials acting as a substrate. Recently, Shang et al.[27] synthesized graphene NS supported ultrafine metal NPs encapsulated by thin mesoporous SiO$_2$ layers. However, in our experiment, because of the large pores of ZrO$_2$−SiO$_2$ with
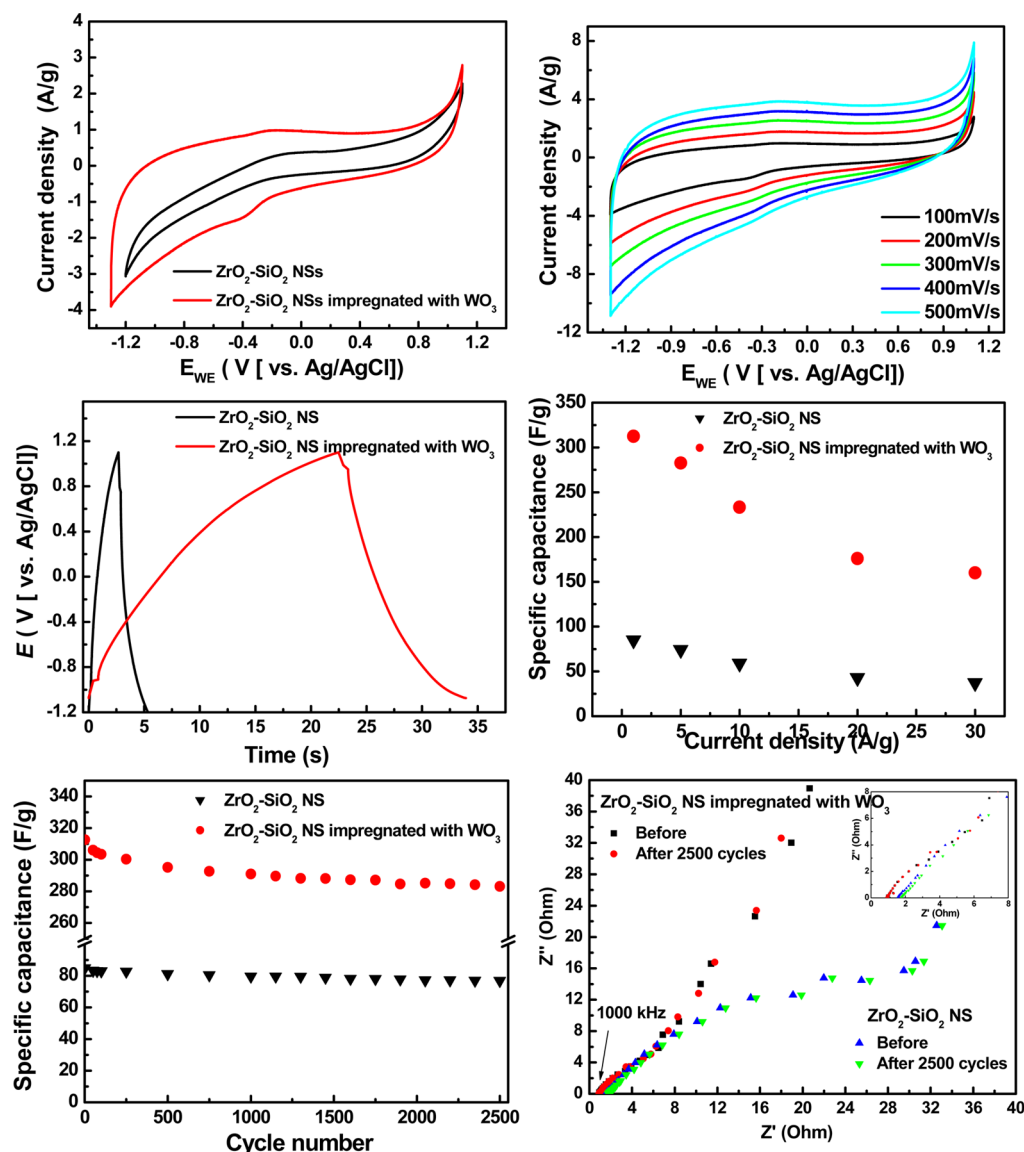
Figure 5. (a) Cyclic voltammetry (CV) curves of porous ZrO_2-SiO_2 NSs impregnated with WO_3 NPs electrodes and ZrO_2-SiO_2 NSs at 100 mV/s and (b) Cyclic voltammograms of the ZrO_2-SiO_2 NSs with ultrasmall WO_3 NPs at different scan rates from 100 to 500 mV/s in 2 M KCl electrolyte. (c) Galvanostatic charging/discharging behaviors of the ZrO_2-SiO_2 NSs with ultrasmall WO_3 NPs and ZrO_2-SiO_2 NSs at a constant current density 30 A/g. (d) Specific capacitance of the ZrO_2-SiO_2 NSs with ultrasmall WO_3 NPs and ZrO_2-SiO_2 NSs electrodes in the range of current density 1−30 A/g in 2 M KCl electrolyte. (e) Cycling life of the ZrO_2-SiO_2 NSs with ultrasmall WO_3 NPs and ZrO_2-SiO_2 NSs electrode at a constant current density 1 A/g. (f) Nyquist plots of the ZrO_2-SiO_2 NSs with ultrasmall WO_3 NPs electrode before/after 2500 cycles at a current density of 1 A/g in 2 M KCl electrolyte.

approximately 10 nm size, our material maintains the pore structure distinctively after impregnating. The diffraction peaks of porous ZrO2-SiO2 NSs with ultrasmall WO_3 nanoparticles are in good agreement with those of monoclinic WO_3. The diffraction peaks can be indexed as monoclinic WO_3 with lattice constants $a = 7.306$, $b = 7.560$, and $c = 7.692$ Å in agreement with the literature values (JCPDS:72−0677). Compared with the XRD pattern of the porous ZrO_2-SiO_2 NSs on GO (Figure 2a), the peaks of the tetragonal ZrO_2 structure were observed after calcination for the oxidation of the W source (Figure 4a). Moreover, the data may imply that WO_3 is well dispersed within the prepared NSs on the GO.

The N_2 adsorption−desorption isotherm and pore size distribution of the porous NS with ultrasmall WO_3 NPs is plotted in Figure 4b. The outer curve is the BHJ pore-size distribution of the sample and shows a relatively narrow

distribution with a pronounced peak and a pore size of approximately 2 nm.

To investigate the electrochemical properties of porous ZrO_2-SiO_2 NS with ultrasmall WO_3 NPs, we performed cyclic voltammetry (CV) in a potential range varying from −1.3 to +1.1 V vs Ag/AgCl in the 2 M KCl electrolyte. First, to clarify the effect of WO_3 NPs, the CV of porous ZrO_2-SiO_2 NS electrode was also measured from −1.2 to +1.1 vs Ag/AgCl in the same electrolyte. Figure 5a shows the CV curves of the porous ZrO_2-SiO_2 NS and porous ZrO_2-SiO_2 NS with ultrasmall WO_3 NP electrodes at a scan rate of 100 mV/s. The CV curve of the ZrO_2-SiO_2 NS with ultrasmall WO_3 NP electrodes has maintained a higher current density than those of porous ZrO_2-SiO_2 NS electrode in a wide potential range. The CV curve of the porous ZrO_2-SiO_2 NS with ultrasmall WO_3 NP electrode had asymmetric redox peak in the region

near −0.2 V, which was not observed in the CV curve of the ZrO_2−SiO_2 NS electrode. This indicates that the electrochemical redox reaction for the capacitance characteristics of ZrO_2−SiO_2 NS with ultrasmall WO_3 NPs has occurred not only because of the surface area but also because of the existence of WO_3 NPs. The porous ZrO_2−SiO_2 NSs on GO with 3.6 nm pore size have a higher surface area (515.19 m^2/g) than that of the highly ordered porous ZrO_2−SiO_2 NS with ultrasmall WO_3 NPs and 2 nm pore size (123.82 m^2/g). Figure 5b shows the CV curves of ZrO_2−SiO_2 NS with ultrasmall WO_3 NP electrode obtained at scan rates varying from 100 to 500 mV/s in the 2 M KCl electrolyte. It is important to note that the CVs of the highly ordered porous ZrO_2−SiO_2 NS with ultrasmall WO_3 NP electrode preserved their shape and were not significantly affected by the change in the CV scan rate. All the Faraday curves are highly electrochemically reversible at a high scan rate of 500 mV/s, indicating the occurrence of the Faraday redox reaction in the 2 M KCl electrolyte.[37] In addition, as the scan rate increases from 100 to 500 mV/s, a cathodic peak current appeared at approximately −0.42 V vs Ag/AgCl and an anodic peak current at approximately −0.22 V vs Ag/AgCl; these currents were directly proportional to the CV scan rate. The obtained results indicate that the highly ordered porous ZrO_2−SiO_2 NS impregnated with WO_3 NP electrode behaves as a pseudocapacitor within the potential window varying from −1.3 to +1.1 V.

Figure 5c shows the first charge−discharge profiles of the highly ordered porous ZrO_2−SiO_2 NS with ultrasmall WO_3 NP and ZrO_2−SiO_2 NS electrodes between −1.2 and 1.1 V (vs Ag/AgCl) at a galvanostatic current density of 30 A/g in the 2 M KCl electrolyte. The shape of the charge/discharge curve of the ZrO_2−SiO_2 NS with ultrasmall WO_3 NP electrode presents the typical pseudocapacitive behavior; an IR drop was observed at the beginning of the discharge curve, which is in agreement with the CV result. In contrast, the porous ZrO_2−SiO_2 NS electrode shows a relatively symmetric triangular shape during the charge/discharge processes and has shorter discharge time than those of the ZrO_2−SiO_2 NS with ultrasmall WO_3 NP electrode. From the charge/discharge measurements, the specific capacitance values of the ZrO_2−SiO_2 NS with ultrasmall WO_3 NP and porous ZrO_2−SiO_2 NS electrodes were calculated from eq 1.

The specific capacitance of the ZrO_2−SiO_2 NS with ultrasmall WO_3 NP electrode was approximately 160.1 F/g, which is five times larger than those of the ZrO_2−SiO_2 NSs (37.2 F/g at current density of 30 A/g).

Figure 5d shows the specific capacitance of the highly ordered porous ZrO_2−SiO_2 NS with ultrasmall WO_3 NP and ZrO_2−SiO_2 NS electrodes at currents densities varying from 1 to 30 A/g. The maximum specific capacitance values of the ZrO_2−SiO_2 NS with ultrasmall WO_3 NP and ZrO_2−SiO_2 NS electrodes were 312.6 F/g and 84.9 F/g at a current density of 1 A/g, respectively; their minimum values were 160.1 F/g and 37.2 F/g at a current density of 30 A/g, respectively. The specific capacitance of the ZrO_2−SiO_2 NS electrode was lower than those of the ZrO_2−SiO_2 NS with ultrasmall WO_3 NP electrode. Even though the specific capacitance of the ZrO_2−SiO_2 NS electrodes was significantly decreased as the current density increased, it still remains at 160.1 F/g at a high current density of 30 A/g because of the well-defined ultrasmall WO_3 on the porous ZrO_2−SiO_2 NS. Recently, Jo et al.[38] reported on the mesoporous $WO_{3−x}$/carbon (m-$WO_{3−x}$-C) synthesized by the one-pot soft template approach for electrochemical

capacitors (ECs). The maximum specific capacitance of the $WO_{3−x}$/carbon nanocomposite was reported to be approximately 169 F/g at a scan rate of 1 mV/s. Compared to those of the mesoporous $WO_{3−x}$/carbon, the ZrO_2−SiO_2 NS with ultrasmall WO_3 NP electrode exhibited good rate capability and superior electrochemical capacitance.[38,39]

The electrochemical stabilities were investigated by repeating the charge/discharge test at a current density of 1A/g for 2500 cycles. Figure 5e shows the good cycling stability of both the ZrO_2−SiO_2 NS with ultrasmall WO_3 NP and ZrO_2−SiO_2 NS electrodes. The specific capacitance of the ZrO_2−SiO_2 NS electrode also gradually decreased from the initial 84.9 to 77 F/g after 2500 cycles. The specific capacitance of the ZrO_2−SiO_2 NS with ultrasmall WO_3 NP electrode decreased by approximately 7% during the initial 1000 cycles (from the initial 312.6 to 291 F/g), and decreased slightly and became stable during the next 1500 cycles. After 2500 cycles of the charge−discharge test, both the ZrO_2−SiO_2 NS with ultrasmall WO_3 NP and ZrO_2−SiO_2 NS electrodes exhibited an outstanding cycle stability with capacitance retention values exceeding 90.5 and 90.7%, respectively, as shown in Figure 5e. During the cycling process, ZrO_2−SiO_2 NSs enhanced the structure stability of the ZrO_2−SiO_2 NS with ultrasmall WO_3 NPs as a template and enhanced the electrochemical stability.

To complement the electrochemical stability of the ZrO_2−SiO_2 NS with ultrasmall WO_3 NP electrode, the electrochemical impedance spectroscopy (EIS) measurements were performed from 100 kHz to 0.05 kHz (Figure 5f). The Nyquist plots of the ZrO_2−SiO_2 NS with ultrasmall WO_3 NP electrode maintained their shape before and after 2500 cycles at a current density of 1 A/g in the 2 M KCl electrolyte. The semicircles in the high and intermediate frequency ranges that correspond to the charge transfer resistance (R_{ct}) and inclined lines in the lower frequency range that represents the Warburg resistance (W) related to the electrolyte diffusion process and ion diffusion into electrode are shown in Figure 5f. Before the cycling test, the electrode series resistance (R_e) value indicated a combinational resistance of the ionic resistance of the electrolyte. The intrinsic resistance of the substrate and contact resistance at the active material/current collector interface of both ZrO_2−SiO_2 NS with ultrasmall WO_3 NPs and ZrO_2−SiO_2 NSs were 0.97 and 1.54 Ω, respectively. After 2500 cycles, the R_e value of the ZrO_2−SiO_2 NS with ultrasmall WO_3 NP and ZrO_2−SiO_2 NS electrodes was 1.00 and 1.77 Ω, respectively. It was also found that the charge transfer resistance and constant phase capacitance (CPE) of the ZrO_2−SiO_2 NSs is approximately 18.5 Ω, which is much larger than that of ZrO_2−SiO_2 NS with ultrasmall WO_3 NPs (only 4.2 Ω). On the basis of the electrode series resistance, the electronic conductivity of the ZrO_2−SiO_2 NS with ultrasmall WO_3 NPs was found to be superior to that of the ZrO_2−SiO_2 NS electrode. It indicates that the conductivity of the ZrO_2−SiO_2 NS with ultrasmall WO_3 NP electrode is considerably improved in comparison with the ZrO_2−SiO_2 NS electrode. Therefore, on the basis of the impedance analysis, it is revealed that the ZrO_2−SiO_2 NS with ultrasmall WO_3 NP electrode has superior electrochemical stability and capacitive properties.

4. CONCLUSION

In our system, for improving the surface deterioration of electrode, we used the ZrO_2−SiO_2 sheets using graphene oxide as a template to access electrode substrate. It is well-known that binary composite oxides like ZrO_2- SiO_2 are important to

obtain materials that exhibit chemical, thermal and mechanical stabilities.[31] Moreover, compared with previous reports, utilization of WO_3 NPs as a real active material for capacitance generation was greatly enhanced by distributing WO_3 NPs on the framework wall. The synthesized electrode with about 13 nm thickness and about 10 nm pores, has a maximum value of 313 F/g at current density of 1 A/g and a minimum value of 160 F/g at current density of 30 A/g in the specific capacitance. In addition, when ZrO_2-SiO_2 sheets impregnated with WO_3 nanoparticle electrode cycled up to 2500 cycles, more than 90% of its initial specific capacitance was retained.

■ ASSOCIATED CONTENT

ⓢ Supporting Information

AFM, TEM, BET results. This material is available free of charge via the Internet at http://pubs.acs.org.

■ AUTHOR INFORMATION

Corresponding Author
* E-mail: swkim@ajou.ac.kr.

Author Contributions
†G.H.J. and H.-M.L. contributed equally.

Notes
The authors declare no competing financial interest.

■ ACKNOWLEDGMENTS

■ REFERENCES

(1) Wang, H.; Casalongue, H. S.; Liang, Y.; Dai, H. Ni(OH)$_2$ Nanoplates Grown on Graphene as Advanced Electrochemical Pseudocapacitor Materials. *J. Am. Chem. Soc.* **2010**, *132*, 7472−7477.

(2) Nakagawa, H.; Shudo, A.; Miura, K. High-Capacity Electric Double-Layer Capacitor with High-Density-Activated Carbon Fiber Electrodes. *J. Electrochem. Soc.* **2000**, *147*, 38−42.

(3) Mayer, S. T.; Pekala, R. W.; Kaschmitter, J. L. The Aerocapacitor: An Electrochemical Double-Layer Energy-Storage Device. *J. Electrochem. Soc.* **1993**, *140*, 446−451.

(4) Hu, C. C.; Huang, Y. H. Effects of Preparation Variables on The Deposition Rate and Physicochemical Properties of Hydrous Ruthenium Oxide for Electrochemical Capacitors. *Electrochim. Acta* **2001**, *46*, 3431−3444.

(5) Wu, X.; Zeng, Y.; Gao, H.; Su, J.; Liu, J.; Zhu, Z. Template Synthesis of Hollow Fusiform RuO$_2$·xH$_2$O Nanostructure and Its Supercapacitor Performance. *J. Mater. Chem. A* **2013**, *1*, 469−472.

(6) Liu, D.; Wang, X.; Wang, X.; Tian, W.; Liu, J.; Zji, C.; He, D.; Bando, Y.; Goldberg, D. Ultrathin Nanoporous Fe$_3$O$_4$−Carbon Nanosheets with Enhanced Supercapacitor Performance. *J. Mater. Chem. A* **2013**, *1*, 1952−1955.

(7) Xu, H.; Zhuang, J. X.; Li, J. L.; Zhang, J. L.; Lu, H. L. Liquid Precipitation Synthesis of Co$_3$O$_4$ for High-Performance Electrochemical Capacitors. *Ionics* **2014**, *20*, 489−494.

(8) Vijayakumar, S.; Nagamuthu, S.; Muralidharan, G. Supercapacitor Studies on NiO Nanoflakes Synthesized Through a Microwave Route. *ACS Appl. Mater. Interface* **2013**, *5*, 2188−2196.

(9) Chol, B. G.; Yang, M.; Jung, S. C.; Lee, K. G.; Kim, J. G.; Park, H.; Park, T. J.; Lee, S. B.; Han, Y. K.; Huh, Y. S. Enhanced Pseudocapacitance of Ionic Liquid/Cobalt Hydroxide Nanohybrids. *ACS Nano* **2013**, *7*, 2453−2460.

(10) Zhu, Y.; Murali, S.; Stoller, M. D.; Ganesh, K. J.; Cai, W.; Ferreira, P. J.; Pirkle, A.; Wallace, R. M.; Cychosz, K. A.; Thommes, M.; Su, D.; Stach, E. A.; Ruoff, R. S. Carbon-Based Supercapacitors Produced by Activation of Graphene. *Science* **2011**, *332*, 1537−1541.

(11) Lee, J. W.; Hall, A. S.; Kim, J. D.; Mallouk, Y. E. A Facile and Template-Free Hydrothermal Synthesis of Mn$_3$O$_4$ Nanorods on Graphene Sheets for Supercapacitor Electrodes with Long Cycle Stability. *Chem. Mater.* **2012**, *24*, 1158−1164.

(12) Liang, R.; Cao, H.; Qian, D. MoO$_3$ Nanowires as Electrochemical Pseudocapacitor Materials. *Chem. Commun.* **2011**, *47*, 10305−10307.

(13) Yu, G.; Hu, L.; Liu, N.; Wang, H.; Vosgueritchian, M.; Yang, Y.; Cui, Y.; Bao, Z. Enhancing the Supercapacitor Performance of Graphene/MnO$_2$ Nanostructured Electrodes by Conductive Wrapping. *Nano Lett.* **2011**, *11*, 4438−4442.

(14) Cheng, Q.; Tang, J.; Ma, J.; Zhang, H.; Shinya, N.; Qin, L. C. Graphene and Carbon Nanotube Composite Electrodes for Supercapacitors with Ultra-High Energy Density. *Phys. Chem. Chem. Phys.* **2011**, *13*, 17615−17624.

(15) Wang, G.; Zhang, L.; Zhang, J. A Review of Electrode Materials for Electrochemical Supercapacitors. *Chem. Soc. Rev.* **2012**, *41*, 797−828.

(16) Chen, S.; Zhu, J.; Wang, X. One-Step Synthesis of Graphene−Cobalt Hydroxide Nanocomposites and Their Electrochemical Properties. *J. Phys. Chem. C* **2010**, *114*, 11829−11834.

(17) Qi, Y.; Zhang, H.; Du, N.; Yang, D. Highly Loaded CoO/Graphene Nanocomposites as Lithium-Ion Anodes with Superior Reversible Capacity. *J. Mater. Chem. A* **2013**, *1*, 2337−2342.

(18) Yan, J.; Fan, Z.; Sun, W.; Ning, G.; Wei, T.; Zhang, Q.; Zhang, R.; Zhi, L.; Wei, F. Advanced Asymmetric Supercapacitors Based on Ni(OH)$_2$/Graphene and Porous Graphene Electrodes with High Energy Density. *Adv. Funct. Mater.* **2012**, *22*, 2632−2641.

(19) Subramani, K.; Jeyakumar, D.; Sathish, M. Manganese Hexacyanoferrate Derived Mn$_3$O$_4$ Nanocubes-Reduced Graphene Oxide Nanocomposites and their Charge Storage Characteristics in Supercapacitors. *Phys. Chem. Chem. Phys.* **2014**, *16*, 4952−4961.

(20) Chen, S.; Zhu, J.; Wu, X.; Han, Q.; Wang, X. Graphene Oxide−MnO$_2$ Nanocomposites for Supercapacitors. *ACS Nano* **2010**, *4*, 2822−2830.

(21) He, G.; Li, J.; Chen, H.; Shi, J.; Sun, X.; Chen, S.; Wang, X. Hydrothermal Preparation of Co$_3$O$_4$@Graphene Nanocomposite for Supercapacitor with Enhanced Capacitive Performance. *Mater. Lett.* **2012**, *82*, 61−63.

(22) Sung, D. Y.; Gunjakar, J. L.; Kim, T. W.; Kim, I. Y.; Lee, Y. R.; Hwang, S. Graphene-Assisted Room-Temperature Synthesis of 2D Nanostructured Hybrid Electrode Materials: Dramatic Acceleration of the Formation Rate of 2D Metal Oxide Nanoplates Induced by Reduced Graphene Oxide Nanosheets. *Chem.—Eur. J.* **2013**, *19*, 7109−7117.

(23) Zhou, X.; Wan, L. J.; Guo, Y. G. Synthesis of MoS$_2$ Nanosheet−Graphene Nanosheet Hybrid Materials for Stable Lithium Storage. *Chem. Commun.* **2013**, *49*, 1838−1840.

(24) Wang, X.; Zhou, X.; Yao, K.; Zhang, J.; Liu, Z. A SnO$_2$/Graphene Composite as a High Stability Electrode for Lithium Ion Batteries. *Carbon* **2011**, *49*, 133−139.

(25) Lee, Y. F.; Chang, K. H.; Hu, C. C.; Lee, Y. H. J. Graphene: A Novel Template for Controlling the Microstructures of Mesoporous Silica. *J. Mater. Chem.* **2011**, *21*, 14008−14012.

(26) Guardia, L.; Garcia, F. S.; Paredes, J. I.; Fernandez, P. S.; Rozada, R.; Merino, F.; Alonso, A. M.; Tascon, J. M. D. Synthesis and Characterization of Graphene−Mesoporous Silica Nanoparticle Hybrids. *Microporous Mesoporous Mater.* **2012**, *160*, 18−24.

(27) Shang, L.; Bian, T.; Zhang, B.; Zhang, D.; Wum, L. Z.; Tung, C. H.; Yin, Y.; Zhang, T. Graphene-Supported Ultrafine Metal Nanoparticles Encapsulated by Mesoporous Silica: Robust Catalysts for Oxidation and Reduction Reactions. *Angew. Chem., Int. Ed.* **2014**, *53*, 250−254.

(28) Li, X.; Qi, W.; Mei, D.; Sushko, M. L.; Aksay, I.; Liu, J. Functionalized Graphene Sheets as Molecular Templates for

Controlled Nucleation and Self-Assembly of Metal Oxide-Graphene Nanocomposites. *Adv. Mater.* **2012**, *24*, 5136−5141.

(29) Wei, W.; Liang, H.; Parvez, K.; Zhuang, X.; Feng, X.; Mullen, K. Nitrogen-Doped Carbon Nanosheets with Size-Defined Mesopores as Highly Efficient Metal-Free Catalyst for the Oxygen Reduction Reaction. *Angew. Chem., Int. Ed.* **2014**, *53*, 1570−1574.

(30) Du, J.; Lai, X.; Yang, N.; Zhai, J.; Kisailus, D.; Su, F.; Wang, D.; Jiang, L. Hierarchically Ordered Macro−Mesoporous TiO_2−Graphene Composite Films: Improved Mass Transfer, Reduced Charge Recombination, and Their Enhanced Photocatalytic Activities. *ACS Nano* **2011**, *5*, 590−596.

(31) Yang, S.; Feng, X.; Wang, L.; Tang, K.; Maier, J.; Mullen, K. Graphene-Based Nanosheets with a Sandwich Structure. *Angew. Chem., Int. Ed.* **2010**, *49*, 4795−4799.

(32) Yang, S.; Zhan, L.; Xu, X.; Wang, Y.; Ling, L.; Feng, X. Graphene-Based Porous Silica Sheets Impregnated with Polyethyleneimine for Superior CO_2 Capture. *Adv. Mater.* **2013**, *25*, 2130−2134.

(33) Yan, Y.; Cheng, Q.; Pavlinek, V.; Saha, P.; Li, C. Controlled Synthesis of Mesoporous Carbon Nanosheets and Their Enhanced Supercapacitive Performance. *J. Solid State Electrochem.* **2013**, *17*, 1677−1684.

(34) Ma, Y.; Jia, P.; Li, X.; Liu, N.; Ma, Y. Synthesis of the ZrO_2−SiO_2 Microspheres as a Mesoporous Candidate Material. *J. Porous. Mater.* **2012**, *19*, 1047−1052.

(35) Jiang, Y.; Yang, S.; Ding, X.; Guo, Y.; Bala, H.; Zhao, J.; Yu, K.; Wang, Z. Synthesis and Catalytic Activity of Stable Hollow ZrO_2−SiO_2 Spheres with Mesopores in the Shell Wall. *J. Mater. Chem.* **2005**, *15*, 2041−2046.

(36) Zu, S. Z.; Han, B. H. Aqueous Dispersion of Graphene Sheets Stabilized by Pluronic Copolymers: Formation of Supramolecular Hydrogel. *J. Phys. Chem.C* **2009**, *113*, 13651−13657.

(37) Wang, Y. H.; Wang, C. C.; Cheng, W. Y.; Lu, S. Y. Dispersing WO_3 in Carbon Aerogel Makes an Outstanding Supercapacitor Electrode Material. *Carbon* **2014**, *69*, 287−293.

(38) Jo, C.; Hwang, J.; Song, H.; Dao, A. H.; Kim, Y. T.; Lee, S. H.; Hong, S. W.; Yoon, S.; Lee, J. W. Block-Copolymer-Assisted One-Pot Synthesis of Ordered Mesoporous WO_{3-x}/Carbon Nanocomposites as High-Rate-Performance Electrodes for Pseudocapacitors. *Adv. Funct. Mater.* **2013**, *23*, 3747−3754.

(39) Yoon, S.; Kang, E.; Kim, J. K.; Lee, C. W.; Lee, J. Development of High-Performance Supercapacitor Electrodes Using Novel Ordered Mesoporous Tungsten Oxide Materials with High Electrical Conductivity. *Chem. Commun.* **2011**, *47*, 1021−1023.